

Nanocrystalline tungsten hydrides at high pressures

Thomas Scheler,¹ Feng Peng,² Christophe L. Guillaume,¹ Ross T. Howie,¹ Yanming Ma,² and Eugene Gregoryanz^{1,*}

¹*SUPA, School of Physics and Astronomy and Centre for Science at Extreme Conditions, The University of Edinburgh, Edinburgh, EH9 3JZ, United Kingdom*

²*State Key Lab of Superhard Materials, Jilin University, 130012 Changchun, People's Republic of China*

(Received 3 May 2012; revised manuscript received 9 May 2013; published 30 May 2013)

A combined experimental and theoretical study has been carried out on the synthesis and characterization of tungsten hydride at high pressures. We confirm the synthesis of tungsten monohydride at above 25 GPa and 300 K. At higher pressures, hydrogen content is found to increase and *ab-initio* calculations reveal the formation of overstoichiometric tungsten hydride WH_n with $n \sim 1\frac{1}{3}$. Synchrotron x-ray diffraction and transmission electron microscopy (TEM) measurements demonstrate the formation of a nanocrystalline microstructure upon hydrogenation. TEM micrographs show elongated grains with diameters of ~ 20 nm, a structure similar to nanocrystalline diamond.

DOI: [10.1103/PhysRevB.87.184117](https://doi.org/10.1103/PhysRevB.87.184117)

PACS number(s): 81.40.Vw, 61.05.cp, 68.37.Lp, 31.15.A-

I. INTRODUCTION

The application of extreme conditions, namely, high pressures and temperatures, offers a very general route for synthesizing novel materials and manipulating their physical properties. In the past, this led to several important discoveries, including nanopolycrystalline diamond (NPD),¹ cubic boron nitride (c-BN),² and the highly incompressible nitrides of osmium, iridium, and platinum.^{3,4} Most recently, nanotwinned c-BN was found to be ultrahard, even exceeding the hardness of diamond.⁵ In the past few years, hydrogen compounds and alloys have attracted the renewed attention of researchers due to their potential applications in a hydrogen economy⁶⁻⁸ and implications for the behavior of free hydrogen, such as its elusive metallic state.^{9,10} High-pressure techniques have also been successfully applied to synthesize novel hydrides, e.g., platinum hydride,^{11,12} ϵ_2 -rhenium hydride,¹³ a polymeric phase of silicon tetrahydride at pressures exceeding 1 Mbar,¹⁴ and tungsten hydride.^{15,16} With the exemption of SiH_4 , the aforementioned materials are interstitial metal hydrides in which the hydrogen atoms occupy octahedral or tetrahedral sites in the closed-packed metal host lattice. Most of the known hydride phases of the *d* metals between the Cr-group and Cu-group elements are of this type.¹⁷ Furthermore, none of the metals in this group readily reacts with hydrogen at ambient conditions, and high pressures are necessary to form a hydride under equilibrium conditions.¹⁷ The conditions for the formation of stoichiometric hydrides range from less than 1 GPa (e.g., NiH at 0.6 GPa,¹⁸) to 27 GPa in platinum,¹¹ so far, the highest synthesis pressure observed in this group.

In this paper, we present a combined x-ray diffraction, electron microscopy, and computational study of tungsten hydride at high pressures. We studied the formation, decomposition, and mechanical properties of tungsten hydride synthesized from the elements in a diamond anvil cell up to 115 GPa by x-ray diffraction as well as the microstructure of recovered dehydrogenated tungsten by transmission electron microscopy. The hydrogenation process was found to create a nanocrystalline microstructure. Theoretical *ab initio* calculations predict the formation of tungsten dihydride (WH_2) at pressures above 50 GPa. Although a pure dihydride phase is not observed in experiments, an increase of hydrogen content is

seen above 25 GPa with an emerging occupation of tetrahedral interstitial sites (corresponding to the hydrogen orientation in WH_2). Combined experimental and computational findings suggest the formation of WH_n with $n \sim 1\frac{1}{3}$.

II. METHODS

In four independent runs, we loaded pristine tungsten powder consisting of single crystalline grains, several micrometers in size, together with hydrogen compressed to 2000 bar into symmetric diamond anvil cells. The hydrogen also acted as the pressure-transmitting medium. Even at the highest pressures reached in these experiments, the tungsten sample was always surrounded by excess hydrogen. In three out of four runs, we used diamonds with 250- μm culets, in the fourth run we used 90- μm beveled diamonds to achieve pressures above 1 Mbar. The pressure was determined using the revised hydrostatic ruby scale up to 70 GPa and the calibrated hydrogen vibron shift above 70 GPa. Rhenium foil of 250 μm was used as a gasket material. Gasket holes of around 50% of the culet diameter were drilled using a YAG infrared laser. The final thickness of the gasket was measured to be 25 μm in the case of the larger culets and ~ 15 μm for the bevelled culets. Angle-dispersive x-ray diffraction patterns using microfocused monochromatic synchrotron radiation ($\lambda = 0.4149$ Å) were collected at the beamlines I15 at Diamond Light Source, United Kingdom, and ID09a at European Synchrotron Radiation Facility, France. MAR345, MAR555, and Perkin Elmer flat panel detectors were used for data collection. X-ray diffraction patterns were analyzed using FIT2D,¹⁹ JADE MDI 9, and JANA 2006. TEM samples were prepared by focused ion beam milling and subsequent lift-out and transfer to a copper TEM grid. The finished samples had a thickness of 80–100 nm. TEM data were collected at the Leeds Electron Microscopy And Spectroscopy center, United Kingdom. *Ab initio* calculations were performed using density functional theory within the Perdew Burke Ernzerhof (PBE) parametrization of the generalized gradient approximation (GGA)²⁰ as implemented in the Vienna *ab initio* simulation package (VASP).²¹ The all-electron projector-augmented wave method (PAW)²² was adopted with the PAW potentials taken from the VASP library. The adopted PAW pseudopotentials of tungsten and hydrogen treat *5d*, *6s*, and *1s*

electrons as valence. A cutoff energy of 700 eV and appropriate Monkhorst-Pack k meshes were chosen to ensure that all enthalpy calculations converged to less than 1 meV/atom. Further details can be found in the Supplementary Material.²³

III. HYDROGENATION AND MICROSTRUCTURE

Tungsten is a widely used material in both industry and science. In high-pressure applications it is particularly valued as a pressure calibrant and gasket material.²⁴ In the past, it was widely accepted that tungsten does not react with hydrogen, even at very high pressures, and therefore was frequently used as a sealing material in high-pressure experiments. However, it was reported a few years ago that binary tungsten hydride is formed when compressing pure tungsten to above 25 GPa at room temperature in a dense hydrogen medium.¹⁵ In a recent study of this material, several potentially metastable phases of varying hydrogen content were found,¹⁶ although only tungsten monohydride was observed experimentally. The monohydride is characterized by a hexagonally closed-packed arrangement of the tungsten atoms (spacegroup $P6_3/mmc$) with hydrogen atoms occupying the octahedral interstitial sites. This is equivalent to the NiAs-type structure, which is known for many other hydrides in the d metals as well and is also the one adopted by the hydrides of the same group, MoH²⁵ and CrH.²⁶

In our experimental runs, we observe a reaction between tungsten and hydrogen at 25 GPa with the appearance of new diffraction peaks in addition to bcc tungsten. The new phase can be indexed in the $P6_3/mmc$ space group with an expanded volume per tungsten atom in the unit cell. So far, our observations are identical with earlier reports on tungsten hydride. The synthesis conditions of WH are reminiscent of hcp platinum hydride¹¹ (PtH), which forms at pressures above 27 GPa and room temperature. However, in contrast to PtH, the hydride formation in tungsten progresses very slowly over time and the diffraction pattern of WH exhibits broadened Bragg peaks (see Fig. 1). In one of our experimental runs, we reached pressures of ~ 45 GPa within hours of surpassing synthesis conditions. At this time, the sample has not been completely converted to tungsten hydride and the sharp Bragg peaks of bcc tungsten are still clearly visible (see Fig. 1). For comparison, we include the diffraction pattern of platinum hydride at similar pressures. It is evident that the diffraction peaks of tungsten hydride are considerably broadened compared to both its parent metal and another hydride synthesized under nearly identical conditions. While increasing pressure seems to accelerate the transformation process, with time, the whole sample fully transforms into the hydride also at constant pressures. In one of the experimental runs the sample was left at a pressure of 38 GPa for one month. Afterwards, the whole sample was hydrogenated and no sign of bcc tungsten was detected. Laser heating has also been shown to accelerate the transition into the hydride phase.¹⁶ On decompression, tungsten hydride was found to be stable to pressures far below synthesis conditions. We observed the decomposition reproducibly at pressures between 8 and 9 GPa. The slow progression of the hydrogenation process, its acceleration upon heating, and the large hysteresis effect in decomposition suggest the presence of a kinetic energy barrier hindering the

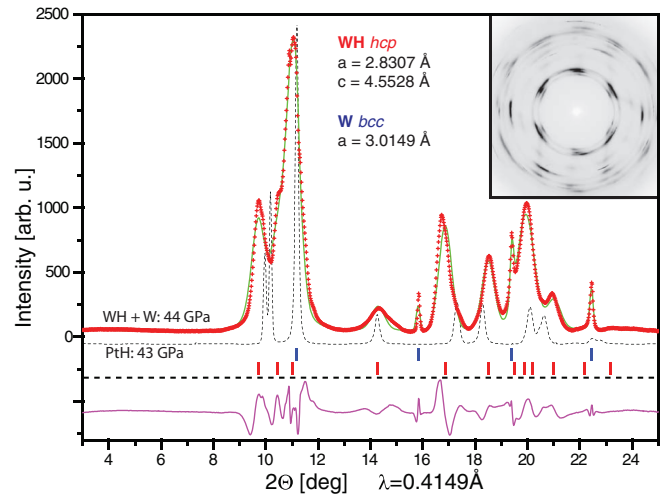


FIG. 1. (Color online) Powder x-ray diffraction spectrum of tungsten hydride at 44 GPa (inset shows 3D diffraction pattern). The green line denotes the result from a LeBail fit. Tick marks indicate peak positions for cubic W (upper, blue) and hexagonal WH (lower, red). The diffraction spectrum of platinum hydride at 43 GPa is added for comparison¹¹ (grey dashed line). Note the difference in peak width. PtH forms under similar conditions as WH and also exhibits the hcp structure.

formation at lower pressures and faster hydrogenation. We found that dehydrogenated tungsten still exhibits broadened Bragg peaks compared to its original state.

We recovered such dehydrogenated tungsten samples from the diamond anvil cells and used focused ion beam techniques to prepare transmission electron microscopy (TEM) samples. TEM brightfield and darkfield imaging revealed elongated crystallites with shortest dimensions of below 20 nm [see Figs. 2(a)–2(c)]. The observed structure is similar to that of NPD, which also exhibits elongated crystallites with diameters of 10–20 nm and lengths of up to a few 100 nm.¹ This new form of artificial diamond was reported to be harder than natural single crystalline diamond.¹ Electron diffraction measurements on dehydrogenated tungsten further show that the crystallites are not randomly oriented but follow a preferred orientation [see Fig. 2(d)], which explains the texture in the x-ray diffraction patterns. In a control experiment, we prepared TEM samples from untreated tungsten. Both, TEM micrographs and electron diffraction patterns [see Fig. 2(e)] indicate perfect single crystallinity.

This microstructure can be related to the observed broadening of the diffraction peaks. Peak broadening in x-ray diffraction patterns during high-pressure experiments can be attributed to three different effects: (i) instrument broadening, (ii) strain broadening, and (iii) size broadening. While instrument broadening can be neglected when using modern third generation synchrotron radiation sources, both strain and size broadening contribute to the peak shape. The simple Scherrer formula $L = \frac{K\lambda}{\beta \cos(\Theta)}$ (see, e.g., Ref. 14) connects the peak width to the crystallite size, ignoring, however, any strain contribution. Here, L is the grain size, λ the x-ray wavelength, β the peak width, and Θ the scattering angle of the reflection. K is the empirical Scherrer constant and usually 1.

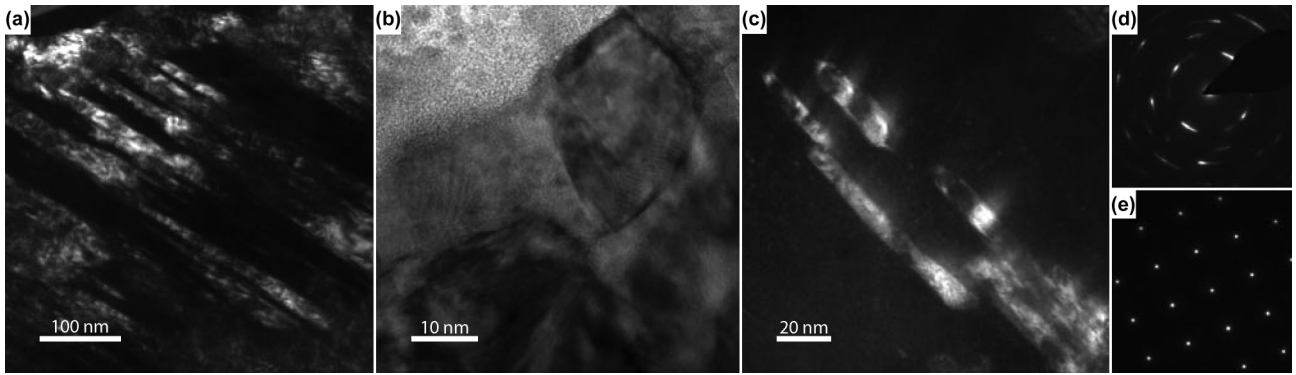


FIG. 2. Transmission electron micrographs of recovered nanocrystalline tungsten. (a) Dark-field image showing an array of elongated crystallites. (b) Bright-field image of crystallites near the surface with their long side perpendicular to the TEM section. (c) In bright-field configuration, dark-field image of small grains inside the sample. The dark-field images allow for a better separation between individual grains, in particular, in a strong absorber such as tungsten. Intensity variations within individual crystallites [best seen in (c)] are mainly due to internal defects, such as prevalent strain. The grain boundaries are clearly visible as abrupt intensity changes. (d) Electron diffraction pattern of nanocrystalline tungsten. (e) Electron diffraction pattern of a single-crystalline control sample. Note the powderlike appearance of diffraction rings in (d).

When comparing the values in Table I for tungsten hydride with the results of the TEM measurements on recovered dehydrogenated tungsten, it is evident that strain plays a significant role at rising pressures (indicated by the decreasing calculated grain size). However, when extrapolating the data in Table I to zero pressure, a grain size comparable to what is found in the TEM images can be derived. It should be emphasized here, that the calculated values at high pressures do not correspond to actual grain sizes. From the emergence of the broad diffraction peaks upon synthesis, we conclude that it is, in fact, the hydrogenation process that leads to the formation of a nanomaterial.

The formation of a nanocrystalline microstructure can be explained by the unusually slow progression of hydride formation. The hydride boundary zone (the volume of material that undergoes hydrogenation at a given time) is therefore very small and the release of boundary strain between pure metal and metal hydride thus leads to the formation of nanometer sized crystallites. It can be expected, that annealing

at high temperatures would lead to a realignment of the grains and the formation of larger crystallites. Indeed, Zaleski-Ejgierd *et al.* seem to have observed this exact effect when laser-heating tungsten hydride to above 1000 K.¹⁶ Room temperature, however, does not appear to have an immediate or a short-term effect on the crystallite size. One of the samples studied by transmission electron microscopy was residing at ambient conditions for several months before TEM-sample preparation, while a different sample was recovered from high pressure only a few days prior to TEM measurements. There were no detectable differences in the microstructure between the two specimens.

IV. EQUATION OF STATE AND STOICHIOMETRY

Decreasing the grain size in materials down to a few tens of nanometers often entails significantly altered material properties, and it is known that, as the grain size decreases, the influence of interface and confinement effects on the properties of a material increases.^{27,28} As a result, a nanostructured material might exhibit increased resistance to plastic deformation²⁹ or different chemical stabilities compared to macroscopic systems.³⁰ In the case of metal hydrides, the grain size has profound impact on (de)hydrogenation processes, the overall hydrogen content and the volume expansion of the metallic host lattice³⁰ due to interface stress between the grains. It was found, for example, in ball milled nanoparticles of vanadium hydride that the hydrogen content depends on the particle size.³¹ These possible nanometric effects make it difficult to compare tungsten hydride to other transition metal hydrides, e.g., in terms of volume expansion as a measure for hydrogen content¹⁷ or when comparing experimental with computational results.

We attempted to fit a Vinet-type equation of state to our x-ray diffraction data resulting in a zero-pressure bulk modulus of near 500 GPa (depending on parameterization). Such extremely low compressibility could be attributed to a size effect of the nanocrystalline microstructure. However, the

TABLE I. Calculated grain size from the widths of the Bragg peaks in tungsten hydride at various pressures using the Scherrer approximation.

P (GPa)	HKL	position (deg)	FWHM (deg)	est. grain size (nm)
9.7	(010)	9.368	0.21	11.5
9.7	(110)	16.251	0.229	11
15.8	(010)	9.439	0.344	7
15.8	(110)	16.301	0.276	9
37.5	(010)	9.512	0.398	6
37.5	(110)	16.432	0.26	9.5
49.7	(010)	9.57	0.41	6
49.7	(110)	16.52	0.304	8
73.7	(010)	9.715	0.428	5.5
73.7	(110)	16.785	0.377	6.5
115	(010)	9.998	0.476	5
115	(110)	17.198	0.454	5.5

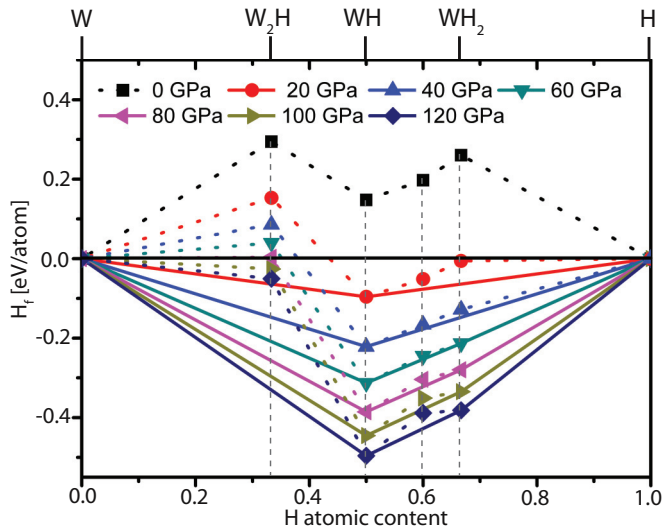


FIG. 3. (Color online) The relative enthalpies of formation per atom with respect to elemental W and molecular H_2 for different WH_n compositions. The convex hulls are shown by solid lines. Dotted lines through the neighboring points residing above the convex hull are guides for the eye.

quality of fit was not convincing, showing deviations at lower and very high pressures. The construction of the equation of state obviously assumes constant stoichiometry throughout the probed pressure range, which unfortunately cannot be guaranteed for metal hydrides. In fact, the volume difference between hydride phase and parent metal is directly used to infer the hydrogen content, assuming no change in compressibility between hydride and metal (see, e.g., Refs. 11, 13, and 17).

We therefore performed *ab initio* calculations to understand hydrogen content and the experimental equation of state. Structure predictions through CALYPSO methodology^{32–34} were performed by fixing the W atomic positions in the hcp lattice, taken from the experimental XRD pattern. We performed structural searches within various stoichiometric compositions WH_n ($n = 0.5, 1.0, 1.5, 2$) with simulation cell sizes of 1–4 formula units (f.u.) at 30 and 60 GPa, respectively. We did not probe higher hydrogen contents since the resulting volumes are too large to fit our experimental data. Our calculations gave convex hulls on the formation enthalpy of various WH_n with respect to elemental W and solid H_2 as shown in Fig. 3 (details can be found in Ref. 23). As expected, at zero pressure, all W-H systems exhibit positive formation enthalpy and cannot form. At 20 and 40 GPa, the monohydride WH is the most stable compound and also the only stoichiometry that can be synthesized, which agrees well with the observed appearance of the hexagonal hydride phase in this pressure range. Interestingly, at a pressure of 60 GPa and above, WH_2 becomes stable against decomposition into $WH + \frac{1}{2}H_2$. Our results are in good agreement with those presented in Ref. 16. However, below 120 GPa, the proposed formation of $P4/nmm$ -structured WH_4 or other phases with even higher hydrogen contents can be excluded based on our experimental observations. At pressures above ~ 220 GPa, when hydrogen enters phase IV, which is characterized by a mixed atomic and molecular state of hydrogen,³⁵ the formation of higher

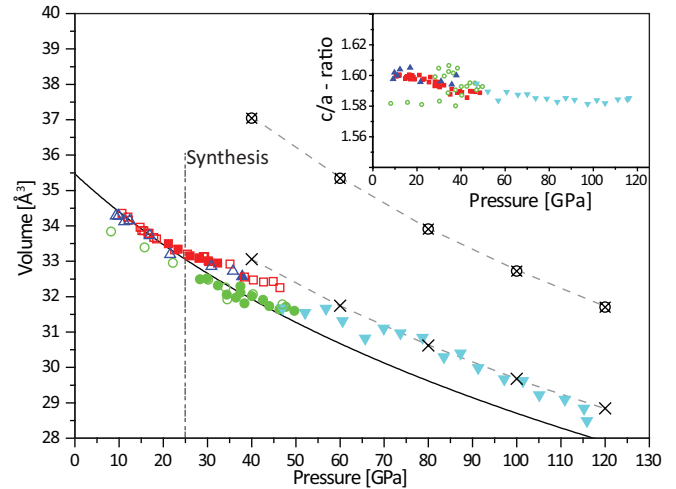


FIG. 4. (Color online) Pressure-volume diagram of tungsten hydride. The solid line indicates the calculated equations of state for WH, the open black circles with crosses EoS-points for WH_2 . Black crosses denote calculated pV data for a fractional mixture of $\frac{2}{3}$ WH and $\frac{1}{3}$ WH_2 or $WH_{3/2}$. The dashed lines are guides to the eye. Smaller symbols are experimental unit-cell volumes from various experimental runs fitted with a hexagonal cell, solid symbols denote data taken on pressure increase, open symbols on pressure decrease. The inset with according symbols shows the c/a ratio. Here, the open green circles show data from a not fully converted sample.

stoichiometries is possible due the absence of the dissociation barrier.

From our calculations, WH stabilizes in the $P6_3/mmc$ space group and WH_2 in the $Pnma$ space group above 50 GPa. For WH, tungsten atoms form a hexagonal closed-packed host matrix with hydrogen atoms occupying the octahedral interstitial sites. In the $Pnma$ structure of WH_2 , the metal atoms are arranged in a slightly distorted hexagonal lattice, very similar to that of WH. In addition to the octahedral sites in the WH-phase, hydrogen atoms also occupy half of the available tetrahedral sites. A transition between these two phases therefore does not require a major rearrangement of the metal host lattice and thus, WH_2 can form in addition to WH at higher pressures. Figure 4 shows the calculated equation of state for WH, WH_2 , and a mixed composition phase of $(1-y)WH + (y)WH_2$ ($y = \frac{1}{3}$), together with our experimental data for comparison. We found that below 25 GPa, the experimental EoS can be satisfactorily explained by pure tungsten monohydride. However, at pressures between 25 and 50 GPa, the experimental volume deviates from the EoS of pure WH, suggesting an additional uptake of hydrogen. It should be noted here, that DFT calculations usually tend to overestimate the volume for a given pressure. Here, we benchmarked the DFT results against experimental findings at pressures below 25 GPa and found very good agreement. We can thus use the comparison between DFT results and experimentally found unit-cell volumes as a measure to derive the hydrogen content. The error of this approach can be estimated to be about 0.1 in the H:M ratio. Above 50 GPa, the observed pressure-volume data show a behavior that is not explained by either pure WH or pure WH_2 . Instead, a

computational mixed-phase model of WH + WH₂ where all octahedral sites and a fraction of the available tetrahedral sites are occupied, can explain the observed behavior. This leads to the conclusion that the reaction $\text{WH} + \frac{1}{2}\text{H}_2 \rightarrow \text{WH}_2$ is initiated and driven by pressure but appears to be halted at pressures above 50 GPa reaching a H:M ratio of $\sim 1\frac{1}{3}$. In other words, once all octahedral sites are filled and sufficient pressure is applied, hydrogen atoms start to occupy a fraction of the tetrahedral sites, forming WH_n with $n \sim 1\frac{1}{3}$. Whether the metallic lattice transforms into the slightly distorted *Pnma* structure or remains perfectly hexagonally oriented is experimentally difficult to address because of the very broad diffraction peaks which allow indexing in either configuration. At the highest pressures reached in this study (115 GPa), the transition to WH₂ is still not complete and tetrahedral occupation seems to saturate at $\sim 17\%$ ($= y/2$, note that for fully stoichiometric WH₂, 50% of the tetrahedral sites are occupied). Even with time (some of our samples resided in this pressure region for several weeks), no higher hydrogen content was reached. In samples that were not fully transformed into the monohydride phase, a slightly smaller volume is measured, indicating a lower hydrogen content, probably due to a deficient filling of the octahedral sites. The nanocrystalline nature of the hydride, however, might add to uncertainty in hydrogen content and atomic ordering. At the same lattice expansion, a larger hydrogen content might be possible due to surface effects in the nanocrystalline grains.

V. SUMMARY

The results presented here are of immediate interest to the field of high-pressure research. The change in microstructure as well as increased hydrogen uptake could have potentially significant consequences since tungsten is often employed as a sealing material in experiments involving pure hydrogen. Due to the higher synthesis pressure of the hydride phase and slower formation kinetics, tungsten gaskets show improved stability at pressures above 1 Mbar compared to rhenium. We hope that the findings presented here will encourage further experimental and theoretical studies on the influence of microstructure and also kinetic effects on the formation and properties of metal hydrides.

ACKNOWLEDGMENTS

The authors would like to thank A. Kleppe from I15 at Diamond Light Source, M. Hanfland from ID09a at the European Synchrotron Radiation Facility and M. Ward from the Leeds Electron Microscopy and Spectroscopy Centre for technical support. The authors further thank O. Degtyareva for useful discussions and T. Strobel for providing unpublished data. This work is supported by a research grant from EPSRC. TS acknowledges financial support from CM-DTC. FP and YM are supported by the National Natural Science Foundation of China under grant No. 11025418. The allocation of beamtime and access to instruments by ESRF, DLS, and LEMAS/LENF is greatly acknowledged.

*Corresponding author: e.gregoryanz@ed.ac.uk

¹T. Irifune, A. Kurio, S. Sakamoto, T. Inoue, and H. Sumiya, *Nature (London)* **421**, 599 (2003).

²R. H. Wentorf, *J. Chem. Phys.* **34**, 809 (1961).

³E. Gregoryanz, C. Sanloup, M. Somayazulu, J. Badro, G. Fiquet, H.-K. Mao, and R. J. Hemley, *Nat. Mater.* **3**, 294 (2004).

⁴A. F. Young, C. Sanloup, E. Gregoryanz, S. Scandolo, R. J. Hemley, and H.-K. Mao, *Phys. Rev. Lett.* **96**, 155501 (2006).

⁵Y. Tian, B. Xu, D. Yu, Y. Ma, Y. Wang, Y. Jiang, W. Hu, C. Tang, Y. Gao, K. Luo, Z. Zhao, L.-M. Wang, B. Wen, J. He, and Z. Liu, *Nature (London)* **493**, 385 (2013).

⁶A. Züttel, *Die Naturwissenschaften* **91**, 157 (2004).

⁷B. Sakintuna *et al.*, *Int. J. Hydrogen Energy* **32**, 1121 (2007).

⁸V. Yartys *et al.*, in *Hydrogen Materials Science and Chemistry of Carbon Nanomaterials*, edited by T. Veziroglu, S. Zaginichenko, D. Schur, B. Baranowski, A. Shpak, and V. Skorokhod (Kluwer Academic Publishers, Dordrecht, The Netherlands, 2004), Vol. 172, pp. 75–104.

⁹N. W. Ashcroft, *Phys. Rev. Lett.* **92**, 187002 (2004).

¹⁰E. Babaev *et al.*, *Phys. Rev. Lett.* **95**, 105301 (2005).

¹¹T. Scheler, O. Degtyareva, M. Marqués, C. L. Guillaume, J. E. Proctor, S. Evans, and E. Gregoryanz, *Phys. Rev. B* **83**, 214106 (2011).

¹²O. Degtyareva, J. E. Proctor, C. L. Guillaume, E. Gregoryanz, and M. Hanfland, *Solid State Commun.* **149**, 1583 (2009).

¹³T. Scheler, O. Degtyareva, and E. Gregoryanz, *J. Chem. Phys.* **135**, 214501 (2011).

¹⁴M. Hanfland, J. E. Proctor, C. L. Guillaume, O. Degtyareva, and E. Gregoryanz, *Phys. Rev. Lett.* **106**, 095503 (2011).

¹⁵H. Kawamura, T. Moriwaki, Y. Akahama, and K. Takemura, in *Proceedings of Joint 20th AIRAPT - 43rd EHPRG International Conference on High Pressure Science and Technology, Karlsruhe, 2005*, edited by E. Dinjus (Karlsruhe Institute of Technology, Karlsruhe, Germany, 2005).

¹⁶P. Zaleski-Ejgierd, V. Labet, T. A. Strobel, R. Hoffmann, and N. W. Ashcroft, *J. Phys.: Condens. Matter* **24**, 155701 (2012).

¹⁷Y. Fukai, *The Metal-Hydrogen System* (Springer Verlag, Berlin, 2005).

¹⁸S. P. Besedin and A. P. Jephcoat, *Rev. High Pressure Sci. Technol.* **7**, 301 (1998).

¹⁹A. P. Hammersley *et al.*, *High Press. Res.* **14**, 235 (1996).

²⁰J. P. Perdew, K. Burke, and M. Ernzerhof, *Phys. Rev. Lett.* **77**, 3865 (1996).

²¹G. Kresse and J. Furthmüller, *Phys. Rev. B* **54**, 11169 (1996).

²²P. E. Blöchl, *Phys. Rev. B* **50**, 17953 (1994).

²³See Supplemental Material at <http://link.aps.org/supplemental/10.1103/PhysRevB.87.184117> for experimental methods and computational details.

²⁴A. Dewaele, P. Loubeyre, and M. Mezouar, *Phys. Rev. B* **70**, 094112 (2004).

²⁵B. Baranowski and K. Bojarski, *Roczn. Chem.* **46**, 525 (1972).

²⁶V. Antonov, A. I. Latynin, and M. Tkacz, *J. Phys.: Condens. Matter* **16**, 8387 (2004).

²⁷M. D. Uchic, D. M. Dimiduk, J. N. Florando, and W. D. Nix, *Science* **305**, 986 (2004).

²⁸G. C. A. M. Janssen, B. R. Pujada, *Appl. Phys. Lett.* **91**, 121913 (2007).

- ²⁹S. Veprek, A. S. Argon, R. F. Zhang, *Philos. Mag.* **90**, 4101 (2010).
- ³⁰M. Fichtner, *Nanotechnology* **20**, 204009 (2009).
- ³¹S.-I. Orimo, F. Kimmerle, and G. Majer, *Phys. Rev. B* **63**, 094307 (2001).
- ³²Y. Wang, J. Lv, L. Zhu, and Y. Ma, *Phys. Rev. B* **82**, 094116 (2010).
- ³³Y. Wang, J. Lv, L. Zhu, and Y. Ma, *Comput. Phys. Commun.* **183**, 2063 (2012).
- ³⁴J. Lv, Y. Wang, L. Zhu, and Y. Ma, *J. Chem. Phys.* **137**, 084104 (2012).
- ³⁵R. T. Howie, C. L. Guillaume, T. Scheler, A. F. Goncharov, and E. Gregoryanz, *Phys. Rev. Lett.* **108**, 125501 (2012).